RSC Sustainability

ROYAL SOCIETY OF CHEMISTRY

PAPER

View Article Online
View Journal | View Issue

Cite this: *RSC Sustainability*, 2024, **2**, 1498

Eggshell incorporated agro-waste adsorbent pellets for sustainable orthophosphate capture from aqueous media†

Bernd G. K. Steiger, Nam T. Bui, Bolanle M. Babalola and Lee D. Wilson *

In this study, granular adsorbents containing varying ratios of torrefied wheat straw (TWS), eggshells (ES), and chitosan (Chi) were prepared, which are referred to as ternary wheat straw composites (TWCs). The TWCs were assessed for mechanical stability during handling in aqueous media and their orthophosphate (P_i) adsorption properties were studied at equilibrium. The characterization of the TWCs employed spectroscopy (IR, solids ^{13}C NMR, PXRD), TGA, and surface area/pore size analysis *via* N_2 gas and dye (4-nitrophenol) adsorption. The BET surface area for the composites increased with greater ES/Chi content from 0.26 $m^2\ g^{-1}$ for C72 (80% TWS content) to 2.2 $m^2\ g^{-1}$ for C22 (20% TWS content; 40% each ES and Chi content). The P_i adsorption properties of selected TWC adsorbents were evaluated *via* the Langmuir, Freundlich, and Sips isotherms at variable pH (4.5, 8.5) and 295 K. The TWCs showed moderate P_i uptake (23–30 mg g^{-1}) at pH 4.5 with a slight decrease (9–12 mg g^{-1}) at pH 8.5 for elevated P_i concentrations. Environmentally relevant P_i concentrations (<5 mg L^{-1}) revealed that TWCs with 20–80% TWS content observed similar uptake (*ca.* 1 mg g^{-1}). This study demonstrates that sustainable composite adsorbents that contain TWS, Chi and ES were modified to yield mechanically stable systems with tailored orthophosphate adsorption properties, especially at low concentrations for neutral or slightly alkaline pH. The proof-of-concept for this adsorbent technology reveals the role of synergistic effects, along with its overall sustainability and scalability, according to a facile synthetic strategy that includes support based on a preliminary cost analysis for these granular adsorbents.

Received 8th November 2023
Accepted 3rd April 2024

DOI: 10.1039/d3su00415e

rsc.li/rscsus

Sustainability spotlight

Orthophosphate (P_i) effluent from industrial and agricultural run-off pose risks to aquatic life through eutrophication and ecosystem disruption. The design of safe and suitable biosorbent technology for controlled removal of P_i near 5 mg L^{-1} at variable pH is urgently needed and environmentally relevant. The proof-of-concept herein relates to the development of sustainable biosorbents with favourable P_i removal across a wide concentration range at variable pH (4.5 and 8.5). We demonstrate the valorization of biomass waste into effective biosorbents for P_i adsorption that address the UN Sustainable Development Goals 6 (water and sanitation) and 9 (industry, innovation and infrastructure). The bioadsorbent technology is highly sustainable, accessible, and scalable, according to a facile synthetic strategy and an initial cost analysis.

1. Introduction

Orthophosphate (P_i) is an essential trace nutrient for all human and plant life. The use of P_i as a key ingredient in fertilizer is directly linked to food security for a growing world population.[1] Currently, a drastic drawback of phosphate rock mining and utilization of P_i is related to the non-sustainable depletion of this non-renewable resource.[2] However, the recovery of P_i from agricultural effluent and aquatic environments will offset eutrophication and other known detrimental environmental effects. Orthophosphate recovery aligns with the UN Sustainable Development Goals (UN SDGs), especially SDG 6 for a clean water supply since the removal of P_i as a target pollutant is of increasing importance.[3] Since access to clean water is essential, reducing contamination and recovery of P_i from secondary sources presents an alternate and sustainable source of P_i. In turn, this will reduce societal dependence on phosphate rock mining, whilst enabling access to secondary and sustainable sources of P_i fertilizer, which can address UN SDG-1 and -2 by reducing poverty and addressing hunger. To this end, adsorption-based removal of P_i offers a facile water treatment strategy, as demonstrated by other studies.[4–9]

Biopolymers are a sustainable and abundant source of potential adsorbent materials. Biopolymers such as chitosan (Chi), cellulosic materials, and their modified forms are

Department of Chemistry, University of Saskatchewan, 110 Science Place – Room 156 Thorvaldson Building, Saskatoon, SK S7N 5C9, Canada. E-mail: lee.wilson@usask.ca

† Electronic supplementary information (ESI) available. See DOI: https://doi.org/10.1039/d3su00415e

versatile adsorbents for the removal of waterborne pollutants.[10,11] Chitinaceous materials derived from crustaceans are appealing adsorbents for anion adsorption due to their cationic nature.[12,13] Although chitosan has been successfully utilized for P_i capture, its widespread adoption has been limited due to the higher material cost of chitosan, along with its relatively low surface area and limited mechanical properties.[6,14,15] To afford more cost-effective materials, composites that contain fillers can offset the chitosan content and improve the physicochemical properties whilst preserving acceptable orthophosphate adsorption properties.[16]

Sustainable and cost-effective precursors for composite formation include agro-wastes (*e.g.*, oat hulls, wheat straw and other mineral waste resources). The use of such waste materials offers valorisation and supports a circular economy. Torrefied wheat straw (TWS) represents a promising agro-waste for conversion into higher value composite adsorbents. Such products can benefit agriculturally intensive regions such as Saskatchewan in Canada, where the use of agro-waste offers a closed-loop strategy to recover P_i, which also serves to address the UN SDG-6. Raw biomass such as lignocellulosic materials (*e.g.*, wheat straw) are often ineffective for anion removal due to the negative surface charge of such biomass. The torrefaction of agro-waste biomass can reduce the amount of polar surface functional groups, along with the improvement of other physical properties. In turn, torrefaction of biomass affords improved properties such as handling, processing, and environmental stability.[11,17–23]

Global egg production steadily rose from 35 million metric tons in 1990 to more than 86 million metric tons in 2021, where a typical eggshell (ES) constitutes *ca.* 10 wt% calcite of the egg bioproduct.[24–26] ES waste from industrial processing plants have limited utility since it contains organic matter that supports pathogen growth. In turn, ES waste is considered a potential biohazard, based on EU regulations.[27] Disposal of ES in landfills is the main disposal strategy for such biomass waste.[28] However, the residual protein content may result in problems for landfilling due to the attraction of vermin and the related effects of microbial buildup on human health. Thus, the innovative use of ES waste is a key solution for alleviating such issues and to increase the environmental sustainability of the egg industry.[29] To address this challenge, researchers have investigated potential ES applications that range from the design of biodiesel catalysts to soil amendment additives due to its calcite content.[24] Recent studies have revealed that ES waste improves soil fertility and its mechanical properties (expansion and stability).[30,31] Plant growth studies on the use of ES mixtures and food waste have demonstrated benefits to both soil pH and plant growth.[32,33] The utility of eggshells as additives for P_i capture and release media has been reported for ES in calcined forms.[34] This research aims to expand the development of sustainable adsorbents for orthophosphate capture and release through the design of composites that require lower energy and less demanding synthesis *via* physical compositing of renewable feedstocks[11,21,22] to afford enhanced P_i capture.

The goal of this study is to explore synergism among components (chitosan, TWS, and ES waste) to prepare a cost-effective and valorized biomass-derived adsorbent in granular form with tailored P_i adsorption properties. This research is anticipated to valorise agro-waste through a circular economy approach to yield adsorbents for controlled Pi removal by providing a sustainable ES upcycling strategy, along with addressing the UN SDGs 1, 2 & 6.

2. Materials and methods

2.1. Materials

Eggshells (ES) were collected after removal of the proteinaceous components. Chitosan (Chi) with low molecular weight and degree of deacetylation (DDA) *ca.* 82%, KBr (FT-IR grade), sulfuric acid (98%+), ascorbic acid (ACS), potassium sodium tartrate tetrahydrate (ACS, 99%+), potassium phosphate (dibasic), potassium antimony(III) tartrate hydrate (99%), antimony molybdate tetrahydrate (99.9%) were purchased from Sigma-Aldrich (Oakville, CA). Potassium phosphate (monobasic, ACS), glacial acetic acid (AcOH; 99.7%), hydrochloric acid (37%) was acquired from Fisher Scientific (Ottawa, CA). Torrefied wheat straw (220 °C) was obtained from the College of Engineering at the University of Saskatchewan. L-Ascorbic acid was obtained from BDH Chemicals (Mississauga, CA). All materials were used as received, unless specified otherwise. Solutions were prepared using MilliPore water (18.2 Mohm·cm resistivity).

2.2. Methods

2.2.1. Pellet preparation. ES biomass was rinsed with several portions of distilled water, twice with Millipore water and oven-dried overnight at 105 °C. The TWS agro-waste biomass and ES were separately ground with a coffee grinder and sieved using size no. 40 (425-micron mesh) U.S.A. Standard Testing Sieve. The agro-waste pellet systems were prepared by combining *ca.* 10 g of sieved materials (according to wt% described in Table 1) in a mortar with mixing, along with 0.2 M acetic acid solution (*ca.* 15 mL) was added to the mixture until a pasty consistency was reached. The resulting product was pressed into plastic moulds (Small Pistol Primer Trays; S&B), as illustrated in Fig. S1 in the ESI.† The product was dried at *ca.* 22 °C overnight, followed by removal of the pellets from the moulds and used without any further modification.

2.2.2. Orthophosphate (P_i) determination. To determine the P_i concentration, an antimony–molybdate solution was employed. Briefly, the antimony–molybdate solution was prepared weekly by mixing with 613 mM ascorbic acid solution (4 mL), 24 mM ammonium molybdate solution (4 mL), 8 mM

Table 1 Composition and acronyms of the prepared pellet systems

	C72	C20	C21	C22
TWS (g)	8.0	6.0	4.0	2.0
ES (g)	1.0	2.0	3.0	4.0
Chi (g)	1.0	2.0	3.0	4.0
$V_{0.2\ M\ AcOH\ solution}$ (mL)	12	13	11	11

antimony potassium tartrate solution (2 mL), and 2.5 M sulfuric acid solution (10 mL). To determine the P_i concentration, an aliquot of P_i solution was added to 3 mL of the prepared antimony–molybdate solution with mixing and colour development (15–20 min) to yield a blue-coloured complex. The absorbance of the solution was measured *via* a UV-vis spectrophotometer at 900 nm (Spectronic 200E, Waltham, MA, USA).[35–37]

2.2.3. Adsorption experiments. For orthophosphate (P_i) adsorption, 1 pellet (*ca.* 25–35 mg) was added to a 4-dram vial with 10 mL of P_i solution. The pH was adjusted to pH 4.5 and pH 8.5 without additional buffer solution. The vials were shaken for 18–24 h on a Scilogex SK-0330-Pro (Rocky Hill, CT, USA), where the adsorption capacity was calculated according to eqn (1):

$$q_e = \frac{C_e - C_0}{m} \times V \quad (1)$$

q_e represents the amount of P_i adsorbed at equilibrium (mg g^{-1}), C_e is the equilibrium concentration (mg L^{-1}) after the adsorption process, and C_0 (mg L^{-1}) is the initial P_i concentration prior to adsorption. V (L) is the total volume and m (g) is the weight of the adsorbent.

The maximum adsorption capacity was evaluated *via* the Sips isotherm, which is also known as the Langmuir–Freundlich isotherm,[11,38,39] according to eqn (2):

$$q_e = \frac{Q_m (K_a C_e)^{1/n}}{1 + (K_a C_e)^{1/n}} \quad (2)$$

Q_m (mg g^{-1}) refers to the maximum monolayer adsorption capacity, K_a is the adsorption constant at equilibrium and n is the heterogeneity constant. The Freundlich and Langmuir isotherm models were also employed (*cf.* Table S3 in ESI† for the model equations).[40,41]

2.2.4. Characterisation. The materials characterisation employed complementary techniques, where the details are outlined in the ESI (*cf.* Section S1†). Thermogravimetric Analysis (TGA) was performed *via* a Q50 TA Instruments TG analyzer (TA Instruments, USA). X-Ray Diffraction (XRD) employed a Bruker-D8 Advance Powder (Billerica, USA) XRD instrument. FT-IR Spectroscopy employed a Bio-Rad FTS-40 (Bio-Rad Laboratories Inc., USA) and spectra were obtained using a diffuse reflectance (DRIFT) configuration. ^{13}C Solids NMR spectra were analysed with a Bruker AVANCE III HD spectrometer at 125.77 Hz with a 4 mm DOTY CP-MAS probe, while the ^{1}H frequency was 500.13 MHz. The surface Area (SA) determination for the dry granular pellets employed an ASAP 2020 surface area and porosity analyzer with N_2 as the backfill gas at −196.2 °C. The surface area (SA) in aqueous media employed a dye adsorption method with *p*-nitrophenol (PNP).[15,42]

The monolayer dye adsorption capacity (Q_m) was obtained from the Sips isotherm (Table 4), which provide an estimate of the adsorbent SA (m^2 g^{-1}) by employing eqn (3).

$$SA = \frac{A_m Q_m L}{N} \quad (3)$$

A_m (m^2 mol^{-1}) is the cross-sectional molecular surface area occupied by PNP (where A_m for the two orientations are: planar is 5.25×10^{-19}; end-on is 2.5×10^{-19} m^2 mol^{-1}), L is Avogadro's number, N is the coverage factor, where N equals 1 for PNP at these conditions.[15,42]

3. Results and discussion

3.1. Characterisation

The characterization of the granular adsorbents as physical blends was accomplished through spectroscopic and gravimetric methods, in addition to the SA determination in the dry and wet states. Fig. 1 with Fig. S2 and S3 in the ESI† outlines the thermogravimetric (TG) decomposition profiles of the composites and raw materials. While all composites observe a low water content (<10%), as indicated by a TG event below 100 °C, while other TG events for the raw materials are observed above 100 °C. The TG profile reveals that ES contains residual organic matter (*ca.* 2.7 wt%) and chitosan exhibits a depolymerization event near 307 °C, whereas TWS decomposed near 332 °C. The TG profile reveals that TWS has low hemi-cellulose content.[43] Decreasing chitosan content occurs for the composites (C22, C21, C20 to C72; Table 1), as revealed by asymmetric peak shapes that correspond to the incremental fraction of TWS and its relative thermal stability, in line with an earlier study.[11]

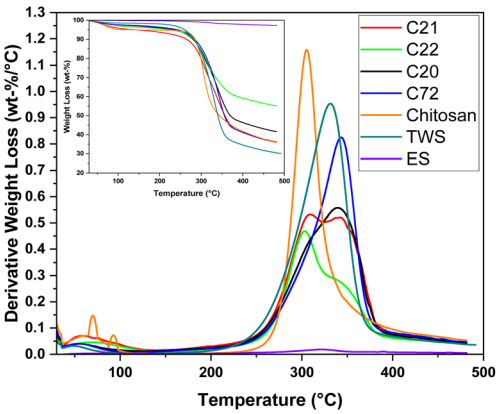

Fig. 1 Differential thermogravimetric (DTG) and thermogravimetric (TG; as inlay) curves of the prepared pellet systems and raw materials.

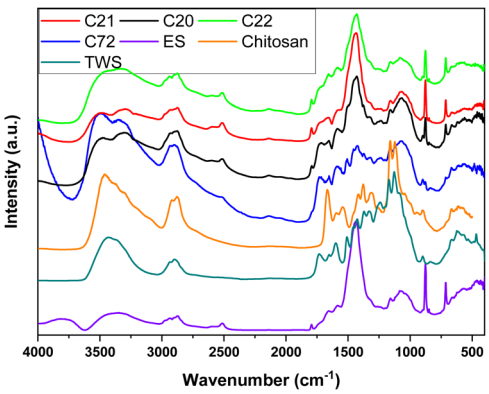

Fig. 2 FT-IR spectra (DRIFT) of the composite pellet systems with a comparison of the raw materials.

FT-IR spectroscopy was employed to identify the chemical groups of the granular adsorbents, as revealed in Fig. 2 and S4 (ESI†). With respect to ES, characteristic bands for CO_3^{-2} are evident at 714 cm^{-1}, 880 cm^{-1} and 1430 cm^{-1}.[44,45] A small, distinct band at 1796 cm^{-1} stems from the eggshells, which is absent for C72 due to its low ES content. The IR band at 2520 cm^{-1} was assigned to organic matter from the eggshell membrane, which contains OH– or $–NH_3^+$ groups, in agreement with the (D)TG results.[46–48] These key IR bands are evident for the composites, where C72 shows low intensity IR bands for eggshells, due to its low ES content (*ca.* 10%, Table 1). The attenuated carbonate band intensity was accounted for by the occurrence of hydrogen bonding (*ca.* 3250 cm^{-1}) and electrostatic interactions with Chi and TWS within the composites, according to spectral shifts and broadening above 3000 cm^{-1} in Fig. 2. As well, the C–H bands around 2800–3000 cm^{-1} were evident for all composites attributed to TWS and chitosan, along with the –OH/–NH bands between 3000 and 3700 cm^{-1}. A characteristic band for TWS was assigned to 1731 cm^{-1} (fatty acid esters), whereas the band at 1647 cm^{-1} (amine bending) likely originates from chitosan. The results herein concur with other reports for biocomposite systems.[11,49–51] The IR results indicate conservation of their original properties (partially amorphous) and adhesive interactions among components such as hydrogen bond formation, as evidence by IR spectral shifts and broadening (*cf.* Fig. 2).[52]

The interactions between ES and acetic acid were assessed by the XRD results to ascertain the presence of the inorganic carbonate signatures (*cf.* Fig. 3). The observed spectra for biopolymer (TWS, Chi) components show highly amorphous peaks that concur with other reports.[49,51,53] Table 2 lists the first 8 XRD bands observed for the eggshells (raw materials) and ternary composites. The observed PXRD lines concur with the expected results[54] for the calcite form of $CaCO_3$ as the main component.[55] The peak intensity roughly corresponds to the incorporated amount of ES (*cf.* Table 1), indicative of retained ES within the composites. The profile for TWS has two main signatures at 16.0° and 21.8°, whereas chitosan has one XRD band at 20.0°. In general, all XRD bands are generally observed for the composite materials with variable band intensity, except for C22, where the ES fraction dominates the observed intensity, in agreement with the ES composition (*cf.* Table 1). The crystallinity of the components does not seem to vary among the raw materials and the composites.[20]

Structural properties of the composites were investigated by employing solid state ^{13}C NMR spectroscopy (*cf.* Fig. 4). At 23.4 and 173 ppm, the signature for C7 (methyl group of CH_3CO) and C8 of the carbonyl amide of chitosan was observed, respectively. In the aromatic region between 125–170 ppm, and spectral features of lignin's or polyphenolics occur at 147 ppm (except in C22). At 104 ppm, prominent bands related to the glucopyranose moiety are evident, while the C3/5 bands appear at 74 ppm. The C2 and C6 signatures appear at 55–57 ppm and 61–65 ppm, which are structurally conserved relative to the pristine biomass. Similarly, relevant signatures for C4 (82–84 ppm) and C5 (88 ppm) are noted for the lignocellulosic materials.

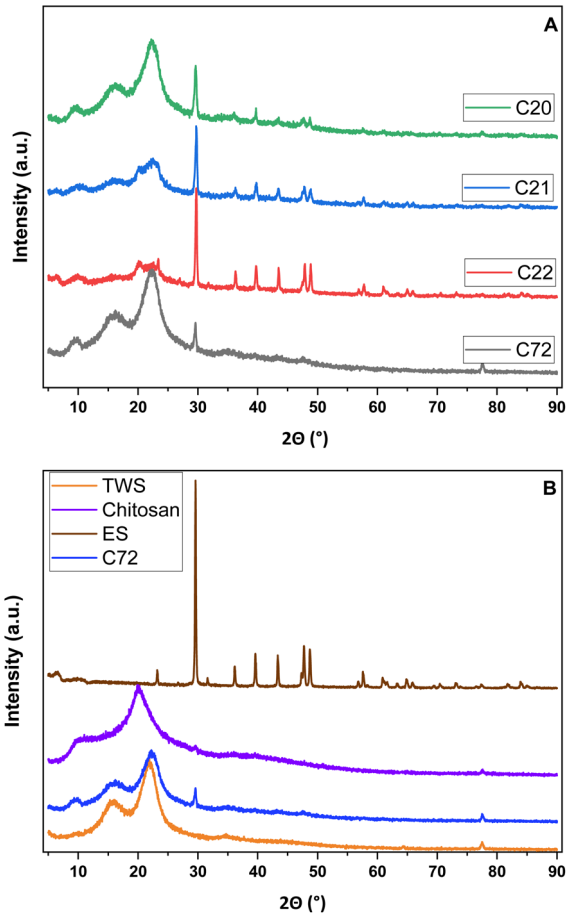

Fig. 3 PXRD spectra of the prepared agro-waste composites (A) and the raw precursor materials for direct comparison with the selected TWC in the form of C72 (B).

Table 2 Identified signatures in the PXRD spectra of the prepared composites (A) and the raw materials (B)

Peak	ES (°)	C72 (°)	C20 (°)	C21 (°)	C22 (°)
1	23.3				—
2	29.7	29.6	29.6	29.6	29.6
3	31.6	—	—	—	31.6
4	36.2	—	36.1	36.1	36.2
5	39.5	—	39.5	39.5	39.7
6	43.4	—	43.4	43.4	43.4
7	47.6	47.7	47.7	47.7	47.8
8	48.6	—	—	48.8	48.8

The accessible surface area (SA) is a key factor that governs the adsorption capacity, including the accessibility of the active sites. In general, a larger SA enhances the uptake of adsorbate. The relationship between the pellet composition and the surface area of the composites (C72, C20–22) were investigated *via* BET analysis, along with a dye-based adsorption method that employs a *p*-nitrophenol (PNP) dye at pH 8.5 (*cf.* Table 3).

For the BET surface area determination, a granular chitosan pellet without additives (ChP) was employed as a control system

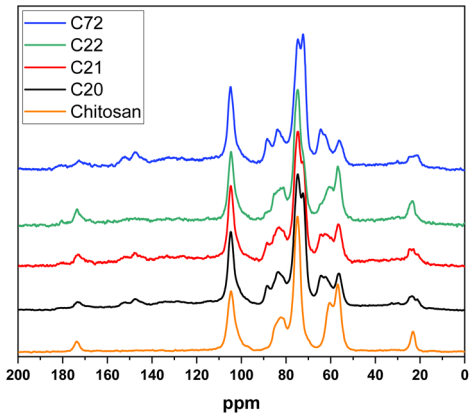

Fig. 4 ^{13}C solids NMR of all four composites and pristine chitosan powder as comparison. Normalized [0, 1].

Table 3 BET surface area (SA) determination of all four composites in comparison to a pure chitosan pellet without addition of eggshells (ChP) at pH 8.5 and 295 K

SA	ChP	C72	C20	C21	C22
BET ($m^2\ g^{-1}$)	0.793	0.256	1.22	1.84	2.16
PNP[a] ($m^2\ g^{-1}$)		79.8	48.2	48.2	25.6
PNP[b] ($m^2\ g^{-1}$)		167.6	101.2	101.2	53.8

[a] End-on orientation. [b] Planar orientation.

to reveal the variation in the accessible SA of chitosan-based pellets where the estimated SA was 0.79 g m^{-2} in the dry state.

The incorporation of greater ES/Chi content (decreasing TWS content) resulted in an increase in the BET surface area from 0.26 $m^2\ g^{-1}$ (C72) to 2.2 $m^2\ g^{-1}$ (C22) as shown in Table 3. In part, this trend can be explained by the morphology of the particles included in the physical composite (*cf.* Fig. 2 in ref. 21 for a comparable pellet system[21]). However, the TWCs can undergo solvent swelling and expansion in aqueous media because of the presence of pores and the polar surface groups due to chitosan. For PNP, the accessible adsorption sites were highest for C72 and lowest for C22, where a decreasing trend was observed. This contrasts with the observed BET surface area (dry state) that can be explained due to swelling and expansion of the TWCs in aqueous media.[16] Additional qualitative information on the pellet stability in aqueous media was obtained at pH 5 and pH 1.85. The TWCs showed no signs of disintegration at pH 5 even after 48 h, whereas C72 was the only stable composite at pH 1.85, while the other pellet systems disintegrated. This is consistent with a previous report for composites that contain kaolinite, which can be attributed to the increased chitosan content.[11]

3.2. Orthophosphate adsorption

3.2.1. Adsorption isotherms. The speciation of orthophosphate depends on the pH conditions, where the favoured P_i species are the mono- and divalent anions. Thus, adsorption studies were performed at pH 4.5 and 8.5, based on the pH stability of the pellets described above. The corresponding isotherm parameters are listed in Tables S1 and S2 (ESI†).

While the Langmuir model assumes homogeneous adsorption sites that are energetically equivalent, the Freundlich model assumes heterogeneous adsorption sites that are non-equivalent.[56,57] The Langmuir–Freundlich combination isotherm (Sips) was employed, in addition to these isotherm models, since it accounts for adsorption onto heterogeneous sites, along with multilayer adsorption. The adsorption results at pH 4.5 and 8.5 are better accounted for by the Sips isotherm model, in accordance with the overall best-fit results ($R^2 > 0.96$) for the composites (*cf.* Table S1†). This trend indicates that the adsorption sites are energetically inequivalent, which concurs with the multi-component nature of these adsorbents, where orthophosphate adopts a monolayer adsorption profile. This trend concurs with a heterogeneity factor (n) that diverges from unity, according to the Sips isotherm model. As well, monolayer adsorption occurs at multiple adsorption sites that are inequivalent (*cf.* Fig. 5).

According to Fig. 5, the composites reveal similar adsorption capacity at equal pH conditions within the estimated experimental errors, whereas the adsorption capacity doubles in value from pH 8.5 to pH 4.5. This indicates that electrostatic interactions between the chitosan and P_i anions highlight key role of active adsorption sites.[58] The adsorption capacity for P_i is attenuated upon going from mono- to divalent anions.[59] While the maximum adsorption capacity at elevated concentrations may be important when attempting to load orthophosphate onto the TWC pellet systems described herein, the P_i

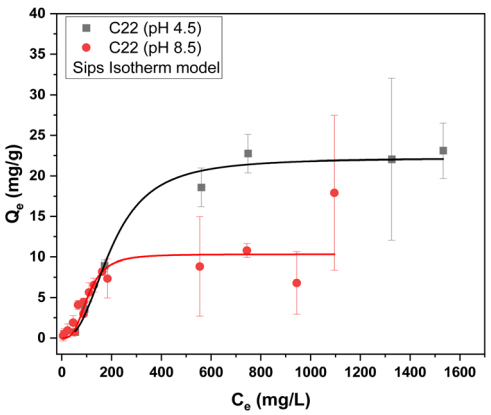

Fig. 5 Orthophosphate adsorption isotherm at pH 4.5 and pH 8.5 at 295 K for C22.

Table 4 Orthophosphate adsorption capacity (Q_m) was taken as single points from the equilibrium isotherm studies at pH 8.5 and 4.5 within the environmentally relevant P_i concentration region (below 5 mg L^{-1}) at 295 K

pH	C72 (mg g^{-1})	C20 (mg g^{-1})	C21 (mg g^{-1})	C22 (mg g^{-1})
8.5	1.13 ± 0.12	1.11 ± 0.12	1.00 ± 0.05	0.63 ± 0.22
4.5	0.98 ± 0.45	0.79 ± 0.32	0.98 ± 0.14	0.68 ± 0.38

Table 5 Comparison across a variety of adsorbents for phosphate capture with emphasis on lower P_i concentrations

	Q_e (mg g^{-1})	Concentration of P_i (mg L^{-1})	pH
Fe–zeolite-A[60]	18.8	4.725	5
Magnetic Fe–oxide[61]	10.9	2–20	2–6
Iron-modified biochar[62]	2–3	0–100	6–5
MIL-101(Al)–CS[63]	49.8	30	3–10
Chitosan–La beads[64]	107.7	50	4
SP–Zr–La[65]	23.5	30	3
$La_2O_2CO_3/\gamma$-Fe_2O_3[66]	0.14	5–100	6.5
$CaCl_2$–buckwheat biochar[67]	75.3	5–1000	7
ES–bentonite[68]	55.7	15–100	3
$Fe(OH)_3$@CNF[69]	142.9	10	4.5
Oh50–furfural[58]	4.9/1.1[a]	0–300	4.75/8.5
MGPA-3 hydrogel[70]	38.8	10–150	6
ES–TWS composites (this study)	20–30/1[a]	5–1200	4.5

[a] 1 mg g^{-1} was attained at *ca.* 5 mg L^{-1} P_i

concentration below 5 mg L^{-1} occurs at environmentally relevant conditions. Hence, a closer look at the singular data determined from the isotherm at 5 mg L^{-1} P_i was employed to gain insight on the P_i uptake for such environmental conditions (*cf.* Table 4).

For P_i capture from effluent run-off at low P_i concentration (up to 5 mg L^{-1}) suggest that C72 or C21 can be effectively deployed (*cf.* Table 4). There is no appreciable difference of the uptake at the selected P_i concentration, based on the estimated experimental errors. A comparison of the estimated adsorption capacities obtained, along with other materials selected from the literature are listed in Table 5.

Various adsorbents (*e.g.*, $Fe(OH)_3$@CNF, chitosan–La beads, MGPA-3 hydrogel) display greater maximum adsorption capacities at relatively low P_i conditions. However, the facile physical blending employed to prepare the granular adsorbents herein bypass the need for more demanding and complex synthetic procedures. In turn, the preparation of the TWCs exemplifies a facile and green synthetic strategy. Furthermore, granular adsorbents possess advantages due to the facile ability to easily separate from aqueous media after the adsorption process, in contrast with powdered adsorbents due to their greater surface area and dispersal in aqueous media.

The adsorption capacity (Q_e; mg g^{-1}), was employed as a measure of adsorbent efficiency. As well, Q_e can provide a measure of the unit cost and the sustainability of the pellet systems.[11] The cost analysis herein accounts for the direct cost of the raw materials, but it does not account for other unit operations in the process (*e.g.*, labour, energy inputs, drying of eggshells and water supply required for washing and cleaning). Based on Table 6, a four-fold cost benefit or adsorption efficiency was observed when C72 was employed, in contrast to C22. The C72 composite system has the highest TWS content (80%) was assessed for the removal of P_i from aqueous solution. Unsurprisingly, the TWC with the highest content of TWS has the least material input cost to prepare this composite, since it employs the lowest content of Chi. The latter represents the more costly component of the TWC adsorbent. It is noteworthy that the reduced chitosan content does not negatively impact the P_i adsorption capacity, even at low P_i concentrations (5 mg L^{-1}). This further highlights the synergistic adsorption properties among the components for this ternary composite system.[16,23]

Table 6 Cost analysis illustration that shows the cost and adsorption sustainability metrics of the pellet systems for orthophosphate adsorption at pH 4.5 and 295 K

Sample ID	Q_m, $H_2PO_4^-$ (g kg^{-1})	Adsorbent cost (USD per kg)	Q_m, $H_2PO_4^-$/cost (g per USD)
C72	0.98	3.15	0.31
C20	0.79	6.16	0.13
C21	0.98	9.17	0.11
C22	0.68	12.17	0.06

Raw materials[a]	US$ per kg
Eggshell	0.36
Wheat straw	0.15
Acetic acid	1.50
Chitosan	30

[a] Estimates obtained from **https://www.Alibaba.com** and **https://www.exportersindia.com**; where the currency exchange rate 06-11-2023 was applied.

4. Conclusions

Four distinct granular adsorbents were prepared for the uptake of orthophosphate (P_i) with variable TWS, ES and Chi content. As well, the physicochemical properties of the composites were characterized. The adsorption capacity approximately doubled for monovalent P_i when compared to the divalent anion (*ca.* 20–30 mg g^{-1} at pH 4.5 *vs.* 10–12 mg L^{-1} at pH 8.5), the relative uptake at low P_i concentration (5 mg L^{-1}) was similar across the TWCs. A cost evaluation based on material input, along with evaluation of the composite stability under adverse pH conditions (pH 1.85) revealed that C72 was the optimal composite. This TWC contains 80% TWS content that displays the lowest cost per kg of adsorbent, which also displays the highest stability in acidic media.

In summary, this research demonstrated the proof-of-concept related to orthophosphate capture at low P_i concentrations (below 5 mg L^{-1}) for agro-waste composite pellets that were prepared by a facile and sustainable method. Future research will address P_i capture in real water samples with more complex matrices that contain competitive ions, and column adsorption studies in combination with orthophosphate release studies. This research reveals the sustainable utility of such composites as soil amendment materials for tailored agricultural applications.

Author contributions

L. D. W.: conceptualisation, funding, project supervision, & editing; B. G. K. S.: writing, analysis, editing; data collection; N. B.: experimental, analysis, data acquisition. B. M. B.: editing.

Conflicts of interest

The authors have no conflicts to declare.

Acknowledgements

The authors acknowledge that this research was carried out on Treaty 6 Territory and the Homeland of the Métis. As such, we pay our respect to the First Nations and Métis ancestors of this place and reaffirm our relationship with one another. The Saskatchewan Structural Science Centre (SSSC) is acknowledged for providing facilities to conduct this research. Mariam Mir is acknowledged for the BET analysis of the samples reported herein. Dr Richard Evitts is gratefully acknowledged for providing samples of the torrefied wheat straw.

References

1 D. A. C. Manning, Phosphate Minerals, Environmental Pollution and Sustainable Agriculture, *Elements*, 2008, **4**(2), 105–108, DOI: **10.2113/GSELEMENTS.4.2.105**.

2 M. El Wali, S. R. Golroudbary and A. Kraslawski, Circular Economy for Phosphorus Supply Chain and Its Impact on Social Sustainable Development Goals, *Sci. Total Environ.*, 2021, 777, 146060, DOI: **10.1016/j.scitotenv.2021.146060**.

3 UNESCO, in *Water Security and the Sustainable Development Goals*, ed. K. Lim, A. K. Makarigakis, O. Sohn and B. Lee, UNESCO, Paris, 1st edn, 2019.

4 H. Bacelo, A. M. A. Pintor, S. C. R. Santos, R. A. R. Boaventura and C. M. S. Botelho, Performance and Prospects of Different Adsorbents for Phosphorus Uptake and Recovery from Water, *Chem. Eng. J.*, 2020, **381**, 122566, DOI: **10.1016/j.cej.2019.122566**.

5 M. H. Mahaninia and L. D. Wilson, Modular Cross-Linked Chitosan Beads with Calcium Doping for Enhanced Adsorptive Uptake of Organophosphate Anions, *Ind. Eng. Chem. Res.*, 2016, **55**(45), 11706–11715, DOI: **10.1021/acs.iecr.6b02814**.

6 M. H. Mahaninia and L. D. Wilson, Phosphate Uptake Studies of Cross-Linked Chitosan Bead Materials, *J. Colloid Interface Sci.*, 2017, **485**, 201–212, DOI: **10.1016/j.jcis.2016.09.031**.

7 J. Jang and D. S. Lee, Effective Phosphorus Removal Using Chitosan/Ca-Organically Modified Montmorillonite Beads in Batch and Fixed-Bed Column Studies, *J. Hazard. Mater.*, 2019, **375**(April), 9–18, DOI: **10.1016/j.jhazmat.2019.04.070**.

8 E. Priya, S. Kumar, C. Verma, S. Sarkar and P. K. Maji, A Comprehensive Review on Technological Advances of Adsorption for Removing Nitrate and Phosphate from Waste Water, *Journal of Water Process Engineering*, 2022, **49**, 103159, DOI: **10.1016/j.jwpe.2022.103159**.

9 B. Liu, S. Gai, Y. Lan, K. Cheng and F. Yang, Metal-Based Adsorbents for Water Eutrophication Remediation: A Review of Performances and Mechanisms, *Environ. Res.*, 2022, **212**, 113353, DOI: **10.1016/j.envres.2022.113353**.

10 A. M. Omer, R. Dey, A. S. Eltaweil, E. M. Abd El-Monaem and Z. M. Ziora, Insights into Recent Advances of Chitosan-Based Adsorbents for Sustainable Removal of Heavy Metals and Anions, *Arabian J. Chem.*, 2022, **15**(2), 103543, DOI: **10.1016/j.arabjc.2021.103543**.

11 B. G. K. Steiger, Z. Zhou, Y. A. Anisimov, R. W. Evitts and L. D. Wilson, Valorization of Agro-Waste Biomass as Composite Adsorbents for Sustainable Wastewater Treatment, *Ind. Crops Prod.*, 2023, **191**, 115913, DOI: **10.1016/j.indcrop.2022.115913**.

12 K. J. Fahnestock, M. S. Austero and C. L. Schauer, Natural Polysaccharides: From Membranes to Active Food Packaging, in *Biopolymers*, Wiley Online Books, John Wiley & Sons, Inc., Hoboken, NJ, USA, 2011, pp. 59–80, DOI: **10.1002/9781118164792.ch3**.

13 S. Ahmed and S. Ikram, *Chitosan*, ed. S. Ahmed and S. Ikram, John Wiley & Sons, Inc., Hoboken, NJ, USA, 2017. DOI: **10.1002/9781119364849**.

14 J.-F. Leduc, R. Leduc and H. Cabana, Phosphate Adsorption onto Chitosan-Based Hydrogel Microspheres, *Adsorpt. Sci. Technol.*, 2014, **32**(7), 557–569, DOI: **10.1260/0263-6174.32.7.557**.

15 M. H. Mahaninia and L. D. Wilson, Cross-Linked Chitosan Beads for Phosphate Removal from Aqueous Solution, *J. Appl. Polym. Sci.*, 2016, **133**(5), 42949, DOI: **10.1002/app.42949**.

16 M. H. Mohamed, I. A. Udoetok and L. D. Wilson, Animal Biopolymer-Plant Biomass Composites: Synergism and Improved Sorption Efficiency, *J. Compos. Sci.*, 2020, **4**(1), 15, DOI: 10.3390/jcs4010015.

17 X. Xu, B. Gao, B. Jin and Q. Yue, Removal of Anionic Pollutants from Liquids by Biomass Materials: A Review, *J. Mol. Liq.*, 2016, **215**, 565–595, DOI: 10.1016/j.molliq.2015.12.101.

18 O. S. Agu, L. G. Tabil, E. Mupondwa and B. Emadi, Torrefaction and Pelleting of Wheat and Barley Straw for Biofuel and Energy Applications, *Frontiers in Energy Research*, 2021, **9**, 699657, DOI: 10.3389/fenrg.2021.699657.

19 M. J. C. van der Stelt, H. Gerhauser, J. H. A. Kiel and K. J. Ptasinski, Biomass Upgrading by Torrefaction for the Production of Biofuels: A Review, *Biomass Bioenergy*, 2011, **35**, 3748–3762, DOI: 10.1016/j.biombioe.2011.06.023.

20 X. Bai, G. Wang, Y. Sun, Y. Yu, J. Liu, D. Wang and Z. Wang, Effects of Combined Pretreatment with Rod-Milled and Torrefaction on Physicochemical and Fuel Characteristics of Wheat Straw, *Bioresour. Technol.*, 2018, **267**, 38–45, DOI: 10.1016/j.biortech.2018.07.022.

21 Y. A. Anisimov, B. G. K. Steiger, D. E. Cree and L. D. Wilson, Moisture Content and Mechanical Properties of Bio-Waste Pellets for Fuel and/or Water Remediation Applications, *J. Compos. Sci.*, 2023, **7**(3), 100, DOI: 10.3390/jcs7030100.

22 M. Solgi, B. G. K. Steiger and L. D. Wilson, A Fixed-Bed Column with an Agro-Waste Biomass Composite for Controlled Separation of Sulfate from Aqueous Media, *Separations*, 2023, **10**(4), 262, DOI: 10.3390/separations10040262.

23 M. H. Mohamed, I. A. Udoetok, M. Solgi, B. G. K. Steiger, Z. Zhou and L. D. Wilson, Design of Sustainable Biomaterial Composite Adsorbents for Point-of-Use Removal of Lead Ions from Water, *Front. Water*, 2022, **4**, 739492, DOI: 10.3389/frwa.2022.739492.

24 S. Aditya, J. Stephen and M. Radhakrishnan, Utilization of Eggshell Waste in Calcium-Fortified Foods and Other Industrial Applications: A Review, *Trends Food Sci. Technol.*, 2021, **115**, 422–432, DOI: 10.1016/j.tifs.2021.06.047.

25 A. Laca, A. Laca and M. Díaz, Eggshell Waste as Catalyst: A Review, *J. Environ. Manage.*, 2017, **197**, 351–359, DOI: 10.1016/j.jenvman.2017.03.088.

26 Statista, Global egg production from 1990 to 2021, https://www.statista.com/statistics/263972/egg-production-worldwide-since-1990/.

27 V. Vandeginste, Food Waste Eggshell Valorization through Development of New Composites: A Review, *Sustainable Mater. Technol.*, 2021, **29**, e00317, DOI: 10.1016/j.susmat.2021.e00317.

28 M. J. Quina, M. A. R. Soares and R. Quinta-Ferreira, Applications of Industrial Eggshell as a Valuable Anthropogenic Resource, *Resour., Conserv. Recycl.*, 2017, **123**, 176–186, DOI: 10.1016/j.resconrec.2016.09.027.

29 M. Waheed, M. Yousaf, A. Shehzad, M. Inam-Ur-Raheem, M. K. I. Khan, M. R. Khan, N. Ahmad, Abdullah and R. M. Aadil, Channelling Eggshell Waste to Valuable and Utilizable Products: A Comprehensive Review, *Trends Food Sci. Technol.*, 2020, **106**, 78–90, DOI: 10.1016/j.tifs.2020.10.009.

30 M. Hamza, K. Farooq, Z. u. Rehman, H. Mujtaba and U. Khalid, Utilization of Eggshell Food Waste to Mitigate Geotechnical Vulnerabilities of Fat Clay: A Micro–Macro-Investigation, *Environ. Earth Sci.*, 2023, **82**(10), 247, DOI: 10.1007/s12665-023-10921-3.

31 U. Zada, A. Jamal, M. Iqbal, S. M. Eldin, M. Almoshaogeh, S. R. Bekkouche and S. Almuaythir, Recent Advances in Expansive Soil Stabilization Using Admixtures: Current Challenges and Opportunities, *Case Studies in Construction Materials*, 2023, **18**, e01985, DOI: 10.1016/j.cscm.2023.e01985.

32 B. Tombarkiewicz, J. Antonkiewicz, M. W. Lis, K. Pawlak, M. Trela, R. Witkowicz and O. Gorczyca, Chemical Properties of the Coffee Grounds and Poultry Eggshells Mixture in Terms of Soil Improver, *Sci. Rep.*, 2022, **12**(1), 2592, DOI: 10.1038/s41598-022-06569-x.

33 A. S. Ma'mor, N. H. Wahida and A. R. Nur Firdaus, The Application of Eggshell and Fruit Peels as Soil Amendment on the Growth Performance and Yield of Corn (Zea Mays L.), *IOP Conference Series: Earth and Environmental Science*, 2023, **1182**(1), 012040, DOI: 10.1088/1755-1315/1182/1/012040.

34 J.-I. Lee, J.-M. Kim, S.-C. Yoo, E. H. Jho, C.-G. Lee and S.-J. Park, Restoring Phosphorus from Water to Soil: Using Calcined Eggshells for P Adsorption and Subsequent Application of the Adsorbent as a P Fertilizer, *Chemosphere*, 2022, **287**, 132267, DOI: 10.1016/j.chemosphere.2021.132267.

35 N. K. Ibnul and C. P. Tripp, A Solventless Method for Detecting Trace Level Phosphate and Arsenate in Water Using a Transparent Membrane and Visible Spectroscopy, *Talanta*, 2021, **225**, 122023, DOI: 10.1016/j.talanta.2020.122023.

36 T. Okazaki, H. Kuramitz, N. Hata, S. Taguchi, K. Murai and K. Okauchi, Visual Colorimetry for Determination of Trace Arsenic in Groundwater Based on Improved Molybdenum Blue Spectrophotometry, *Anal. Methods*, 2015, **7**(6), 2794–2799, DOI: 10.1039/c4ay03021d.

37 D. J. Venegas-García, B. G. K. Steiger and L. D. Wilson, A Pyridinium-Modified Chitosan-Based Adsorbent for Arsenic Removal via a Coagulation-like Methodology, *RSC Sustainability*, 2023, 1259–1269, DOI: 10.1039/D3SU00130J.

38 R. Sips, On the Structure of a Catalyst Surface, *J. Chem. Phys.*, 1948, **16**(5), 490–495, DOI: 10.1063/1.1746922.

39 S. Kalam, S. A. Abu-Khamsin, M. S. Kamal and S. Patil, Surfactant Adsorption Isotherms: A Review, *ACS Omega*, 2021, **6**(48), 32342–32348, DOI: 10.1021/acsomega.1c04661.

40 H. M. F. Freundlich, Über Die Adsorption in Lösungen, *Zeitschrift für Physikalische Chemie*, 1906, **57**, 385–470.

41 I. Langmuir, The Adsorption of Gases on Plane Surfaces of Glass, Mica and Platinum, *J. Am. Chem. Soc.*, 1918, **40**(9), 1361–1403, DOI: 10.1021/ja02242a004.

42 L. D. Wilson, M. H. Mohamed and J. V. Headley, Surface Area and Pore Structure Properties of Urethane-Based

Copolymers Containing β-Cyclodextrin, *J. Colloid Interface Sci.*, 2011, **357**(1), 215–222, DOI: 10.1016/j.jcis.2011.01.081.

43 T. Emiola-Sadiq, L. Zhang and A. K. Dalai, Thermal and Kinetic Studies on Biomass Degradation via Thermogravimetric Analysis: A Combination of Model-Fitting and Model-Free Approach, *ACS Omega*, 2021, **6**(34), 22233–22247, DOI: 10.1021/acsomega.1c02937.

44 O. Awogbemi, F. Inambao and E. I. Onuh, Modification and Characterization of Chicken Eggshell for Possible Catalytic Applications, *Heliyon*, 2020, **6**(10), e05283, DOI: 10.1016/j.heliyon.2020.e05283.

45 G. Busca and C. Resini, Vibrational Spectroscopy for the Analysis of Geological and Inorganic Materials, in *Encyclopedia of Analytical Chemistry*, Wiley, 2000, DOI: 10.1002/9780470027318.a5612m.

46 M. S. Tizo, L. A. V. Blanco, A. C. Q. Cagas, B. R. B. Dela Cruz, J. C. Encoy, J. V. Gunting, R. O. Arazo and V. I. F. Mabayo, Efficiency of Calcium Carbonate from Eggshells as an Adsorbent for Cadmium Removal in Aqueous Solution, *Sustainable Environ. Res.*, 2018, **28**(6), 326–332, DOI: 10.1016/j.serj.2018.09.002.

47 H. Daraei, A. Mittal, J. Mittal and H. Kamali, Optimization of Cr(VI) Removal onto Biosorbent Eggshell Membrane: Experimental & Theoretical Approaches, *Desalin. Water Treat.*, 2014, **52**(7–9), 1307–1315, DOI: 10.1080/19443994.2013.787374.

48 W. T. Tsai, J. M. Yang, C. W. Lai, Y. H. Cheng, C. C. Lin and C. W. Yeh, Characterization and Adsorption Properties of Eggshells and Eggshell Membrane, *Bioresour. Technol.*, 2006, **97**(3), 488–493, DOI: 10.1016/j.biortech.2005.02.050.

49 P. N. Diagboya, B. I. Olu-Owolabi, F. M. Mtunzi and K. O. Adebowale, Clay-Carbonaceous Material Composites: Towards a New Class of Functional Adsorbents for Water Treatment, *Surf. Interfaces*, 2020, **19**, 100506, DOI: 10.1016/j.surfin.2020.100506.

50 P. N. Diagboya, B. J. Heyde and R.-A. Düring, Efficient Decontamination of Aqueous Glyphosate Using Santa Barbara Amorphous-15 (SBA-15) and Graphene Oxide-SBA-15 Poly-Amidoamine Functionalized Composites, *Chem. Eng. J.*, 2023, **466**, 143263, DOI: 10.1016/j.cej.2023.143263.

51 R. P. Mohubedu, P. N. E. Diagboya, C. Y. Abasi, E. D. Dikio and F. Mtunzi, Magnetic Valorization of Biomass and Biochar of a Typical Plant Nuisance for Toxic Metals Contaminated Water Treatment, *J. Cleaner Prod.*, 2019, **209**, 1016–1024, DOI: 10.1016/j.jclepro.2018.10.215.

52 W. Qiu, M. Vakili, G. Cagnetta, J. Huang and G. Yu, Effect of High Energy Ball Milling on Organic Pollutant Adsorption Properties of Chitosan, *Int. J. Biol. Macromol.*, 2020, **148**, 543–549, DOI: 10.1016/j.ijbiomac.2020.01.171.

53 P. R. Sera, P. N. Diagboya, S. O. Akpotu, F. M. Mtunzi and T. B. Chokwe, Potential of Valourized Moringa Oleifera Seed Waste Modified with Activated Carbon for Toxic Metals Decontamination in Conventional Water Treatment, *Bioresour. Technol. Rep.*, 2021, **16**, 100881, DOI: 10.1016/j.biteb.2021.100881.

54 Y. Zhang, H. Li, Y. Zhang, F. Song, X. Cao, X. Lyu, Y. Zhang and J. Crittenden, Statistical Optimization and Batch Studies on Adsorption of Phosphate Using Al-Eggshell, *Adsorpt. Sci. Technol.*, 2018, **36**(3–4), 999–1017, DOI: 10.1177/0263617417740790.

55 M. A. Rahman and T. Oomori, Structure, Crystallization and Mineral Composition of Sclerites in the Alcyonarian Coral, *J. Cryst. Growth*, 2008, **310**(15), 3528–3534, DOI: 10.1016/j.jcrysgro.2008.04.056.

56 O. Sahu and N. Singh, Significance of Bioadsorption Process on Textile Industry Wastewater, in *The Impact and Prospects of Green Chemistry for Textile Technology*, Elsevier, 2019, pp. 367–416, DOI: 10.1016/B978-0-08-102491-1.00013-7.

57 A. de Sá, A. S. Abreu, I. Moura and A. V. Machado, Polymeric Materials for Metal Sorption from Hydric Resources, in *Water Purification*, Elsevier, 2017, pp. 289–322, DOI: 10.1016/B978-0-12-804300-4.00008-3.

58 B. G. K. Steiger and L. D. Wilson, Pyridinium-Furfuryl-Modified Granular Agro-Waste Adsorbent for Orthophosphate Recovery, *RSC Sustainability*, 2023, **1**, 1540–1546, DOI: 10.1039/D3SU00171G.

59 R.-F. Chen, T. Liu, H.-W. Rong, H.-T. Zhong and C.-H. Wei, Effect of Organic Substances on Nutrients Recovery by Struvite Electrochemical Precipitation from Synthetic Anaerobically Treated Swine Wastewater, *Membranes*, 2021, **11**(8), 594, DOI: 10.3390/membranes11080594.

60 M. Saifuddin, J. Bae and K. S. Kim, Role of Fe, Na and Al in Fe-Zeolite-A for Adsorption and Desorption of Phosphate from Aqueous Solution, *Water Res.*, 2019, **158**, 246–256, DOI: 10.1016/j.watres.2019.03.045.

61 S.-Y. Yoon, C.-G. Lee, J.-A. Park, J.-H. Kim, S.-B. Kim, S.-H. Lee and J.-W. Choi, Kinetic, Equilibrium and Thermodynamic Studies for Phosphate Adsorption to Magnetic Iron Oxide Nanoparticles, *Chem. Eng. J.*, 2014, **236**, 341–347, DOI: 10.1016/j.cej.2013.09.053.

62 D. G. Strawn, A. R. Crump, D. Peak, M. Garcia-Perez and G. Möller, Reactivity of Fe-Amended Biochar for Phosphorus Removal and Recycling from Wastewater, *PLOS Water*, 2023, **2**(4), e0000092, DOI: 10.1371/journal.pwat.0000092.

63 S. Zhang, J. Ding and D. Tian, Incorporation of MIL-101 (Fe or Al) into Chitosan Hydrogel Adsorbent for Phosphate Removal: Performance and Mechanism, *J. Solid State Chem.*, 2022, **306**, 122709, DOI: 10.1016/j.jssc.2021.122709.

64 K. Y. Koh, Z. Chen, S. Zhang and J. P. Chen, Cost-Effective Phosphorus Removal from Aqueous Solution by a Chitosan/Lanthanum Hydrogel Bead: Material Development, Characterization of Uptake Process and Investigation of Mechanisms, *Chemosphere*, 2022, **286**, 131458, DOI: 10.1016/j.chemosphere.2021.131458.

65 W. Du, Y. Li, X. Xu, Y. Shang, B. Gao and Q. Yue, Selective Removal of Phosphate by Dual Zr and La Hydroxide/Cellulose-Based Bio-Composites, *J. Colloid Interface Sci.*, 2019, **533**, 692–699, DOI: 10.1016/j.jcis.2018.09.002.

66 S. Shan, W. Wang, D. Liu, Z. Zhao, W. Shi and F. Cui, Remarkable Phosphate Removal and Recovery from Wastewater by Magnetically Recyclable $La_2O_2CO_3/\gamma$-Fe_2O_3 Nanocomposites, *J. Hazard. Mater.*, 2020, **397**, 122597, DOI: 10.1016/j.jhazmat.2020.122597.

67 F. Pan, H. Wei, Y. Huang, J. Song, M. Gao, Z. Zhang, R. Teng and S. Jing, Phosphorus Adsorption by Calcium Chloride-Modified Buckwheat Hulls Biochar and the Potential Application as a Fertilizer, *J. Cleaner Prod.*, 2024, **444**, 141233, DOI: **10.1016/j.jclepro.2024.141233**.

68 S. Sudhakaran, H. Mahadevan, S. L. Fathima and K. A. Krishnan, Performance of Novel Pillared Eggshell-Bentonite Clay Bio-Composite for Enhanced Phosphate Adsorption from Aqueous Media, *Groundwater for Sustainable Development*, 2023, **22**, 100960, DOI: **10.1016/j.gsd.2023.100960**.

69 G. Cui, M. Liu, Y. Chen, W. Zhang and J. Zhao, Synthesis of a Ferric Hydroxide-Coated Cellulose Nanofiber Hybrid for Effective Removal of Phosphate from Wastewater, *Carbohydr. Polym.*, 2016, **154**, 40–47, DOI: **10.1016/j.carbpol.2016.08.025**.

70 W. Zhang, Y. Wu, H. Chen, Y. Gao, L. Zhou, J. Wan, Y. Li, M. Tang, Y. Peng, B. Wang, H. Wang and S. Sun, Efficient Phosphate Removal from Water by Multi-Engineered PVA/SA Matrix Double Network Hydrogels: Influencing Factors and Removal Mechanism, *Sep. Purif. Technol.*, 2024, **336**, 126261, DOI: **10.1016/j.seppur.2023.126261**.